MntABC and MntH Contribute to Systemic Staphylococcus aureus Infection by Competing with Calprotectin for Nutrient Manganese

Article *in* Infection and immunity · July 2013

Impact Factor: 3.73 · DOI: 10.1128/IAI.00420-13 · Source: PubMed

9 authors, including:

Thomas E Kehl-Fie
University of Illinois, Urbana-Champaign
35 PUBLICATIONS **906** CITATIONS
SEE PROFILE

Allison J Farrand
University of Oklahoma Health Sciences C…
12 PUBLICATIONS **210** CITATIONS
SEE PROFILE

Marguerite Indriati Hood
Boston Children's Hospital
18 PUBLICATIONS **506** CITATIONS
SEE PROFILE

Walter J Chazin
Vanderbilt University
308 PUBLICATIONS **10,540** CITATIONS
SEE PROFILE

Infection and Immunity

MntABC and MntH Contribute to Systemic Staphylococcus aureus Infection by Competing with Calprotectin for Nutrient Manganese

Thomas E. Kehl-Fie, Yaofang Zhang, Jessica L. Moore, Allison J. Farrand, M. Indriati Hood, Subodh Rathi, Walter J. Chazin, Richard M. Caprioli and Eric P. Skaar

Infect. Immun. **2013, 81(9):3395. DOI: 10.1128/IAI.00420-13. Published Ahead of Print 1 July 2013.**

IAI Journals.ASM.org

MntABC and MntH Contribute to Systemic *Staphylococcus aureus* Infection by Competing with Calprotectin for Nutrient Manganese

Thomas E. Kehl-Fie,[a] Yaofang Zhang,[a] Jessica L. Moore,[b,c] Allison J. Farrand,[a] M. Indriati Hood,[a] Subodh Rathi,[b,d,e] Walter J. Chazin,[b,d,e] Richard M. Caprioli,[c,e] Eric P. Skaar[a]

Department of Pathology, Microbiology & Immunology,[a] Department of Chemistry,[b] Mass Spectrometry Research Center,[c] Center for Structural Biology,[d] and Department of Biochemistry,[e] Vanderbilt University School of Medicine, Nashville, Tennessee, USA

During infection, vertebrates limit access to manganese and zinc, starving invading pathogens, such as *Staphylococcus aureus*, of these essential metals in a process termed "nutritional immunity." The manganese and zinc binding protein calprotectin is a key component of the nutrient-withholding response, and mice lacking this protein do not sequester manganese from *S. aureus* liver abscesses. One potential mechanism utilized by *S. aureus* to minimize host-imposed manganese and zinc starvation is the expression of the metal transporters MntABC and MntH. We performed transcriptional analyses of both *mntA* and *mntH*, which revealed increased expression of both systems in response to calprotectin treatment. MntABC and MntH compete with calprotectin for manganese, which enables *S. aureus* growth and retention of manganese-dependent superoxide dismutase activity. Loss of MntABC and MntH results in reduced staphylococcal burdens in the livers of wild-type but not calprotectin-deficient mice, suggesting that these systems promote manganese acquisition during infection. During the course of these studies, we observed that metal content and the importance of calprotectin varies between murine organs, and infection leads to profound changes in the anatomical distribution of manganese and zinc. In total, these studies provide insight into the mechanisms utilized by bacteria to evade host-imposed nutrient metal starvation and the critical importance of restricting manganese availability during infection.

Staphylococcus aureus is a commensal organism that asymptomatically colonizes nearly one-third of the population (1). However, once *S. aureus* breaches the epithelial barrier, the bacterium is capable of infecting nearly every organ despite the robust defenses elaborated by the host (2). This adaptability contributes to the significant morbidity and mortality associated with *S. aureus* infections. The emergence of methicillin- and vancomycin-resistant isolates has compounded the threat of this organism, highlighting the need to identify new therapeutics (3–7). This is of particular importance, as antibiotic resistance is prevalent in both hospital- and community-acquired isolates (4, 6, 8).

Metals are essential for all forms of life due to their critical contributions to protein structure and enzymatic function (9–12). To combat invading pathogens, vertebrates leverage the essentiality of transition metals by restricting their availability, a process termed "nutritional immunity" (10, 13). While the most prominent example of nutritional immunity is the restriction of iron (Fe) by the host, it has recently been discovered that vertebrates also limit manganese (Mn) and zinc (Zn) availability during infection (10, 13–17). In fact, examination of abscesses formed during *S. aureus* infection has revealed that these lesions are Mn and Zn depleted (14). It was subsequently determined that the Mn- and Zn-binding S100 protein calprotectin (CP) is a critical component of this nutrient-withholding response (10, 14, 18, 19). CP-deficient mice fail to remove Mn, but not Zn, from staphylococcal liver abscesses and have higher bacterial burdens during infection (14, 18). CP-deficient mice are also more susceptible to a range of bacterial and fungal pathogens, including *Acinetobacter baumannii*, *Candida albicans*, and *Aspergillus fumigatus* (14, 18, 20–22). Considering the fact that CP binds both Mn and Zn with high affinity, the increased susceptibility of CP-deficient mice to these other pathogens may be due to defects in the sequestration of Mn and/or Zn (21, 23).

CP comprises 40 to 60% of the total cytoplasmic protein in neutrophils and can be found at sites of infection in excess of 1 mg/ml (24, 25). CP is a heterodimer of S100A8 and S100A9 and has two distinct transition metal-binding sites (26–29). One is a canonical S100 protein site composed of three histidine and one aspartic acid side chain, and the other binding site is formed exclusively by histidines (27). Even though both sites are capable of binding Zn with high affinity, the unique S100A9 C-terminal extension enables CP to form a distinctive hexahistidine site capable of binding Mn (27). Metal sequestration is known to be essential for the antimicrobial activity of CP (18, 30). However, the individual contributions of Mn and Zn sequestration have been difficult to determine due to the fact that calprotectin chelates both of these metals. Utilization of CP variants engineered to have altered metal-binding capacity has revealed that the sequestration of both Mn and Zn contributes to the antimicrobial activity of CP (27). These variants also provide a set of tools to assess the bacterial response to Mn and Zn starvation through the use of this biologically relevant metal chelator.

In order to cause disease, successful pathogens such as *S. aureus* must possess mechanisms to circumvent host-imposed Mn and

Received 4 April 2013 Returned for modification 23 April 2013
Accepted 22 June 2013
Published ahead of print 1 July 2013
Editor: S. M. Payne
Address correspondence to Eric P. Skaar, eric.skaar@vanderbilt.edu.
Supplemental material for this article may be found at http://dx.doi.org/10.1128/IAI.00420-13.

doi:10.1128/IAI.00420-13

TABLE 1 PCR primers used in this study

Name	Sequence
MntH K/O 3′ Rev	CCCGGGCAAAGTTAAAAATAAAACCATTAAAATGTTGG
MntH K/O 3′ Fwd	GGGGACAAGTTTGTACAAAAAAGCAGGCTGATGATGGTTATTATGCAGAACCTGAAG
MntH K/O 5′ Fwd	CCCGGGATTATTCATTTTGACTCACCTCTACTTCTTATG
MntH K/O 5′ Rev	GGGGACCACTTTGTACAAGAAAGCTGGGTATCCTCACGTAGCAAAGCATGC
MntC K/O 3′ Rev	ACTGCCCGGGGGAAGCATGAAATAACACGCTGTG
MntC K/O 3′ Fwd	GGGGACAAGTTTGTACAAAAAAGCAGGCTGATGAAATGGTTATTGTAGATAGTATGACGTAG
MntC K/O 5′ Fwd	ACTGCCCGGGACCAACATTTTTAGCCATATCATATAAAATTG
MntC K/O 5′ Rev	GGGGACCACTTTGTACAAGAAAGCTGGGTTTATGAGTAGCACTGACTGTAGTGACCCTAGTC
MntC 5′ Comp	AGTCCATATGAAAAAATTAGTACCTTTATTATTAGCCTTATTACTTC
MntC 3′ Comp	AGTCGGATCCACAGCGTGTTATTTCATGCTTCCG
MntH 5′ Comp	AGTCCATATGAATAATAAACGACATTCAACAAATGAAC
MntH 3′ Comp	AGTCCATATGGTTTTATTTTTAACTTTGTAGTTCTTGGAATGTTTG
MntA RT Left	TCTAGATGAGCCGTTTGTCG
MntA RT Right	GCTTTTGATAGATCATGGTGGA
MntH RT Left	AATTCGATCATCGCAGTTCA
MntH RT Right	GCCACCTTGCATTGATGTTA

Zn starvation. One such mechanism is the expression of dedicated metal uptake systems. In this regard, Mn and Zn uptake systems have been shown to contribute to the pathogenesis of a number of bacterial species, including *Campylobacter jejuni*, *Salmonella enterica*, *Haemophilus ducreyi*, uropathogenic *Escherichia coli*, *Brucella abortus*, *Yersinia pestis*, *Streptococcus pneumoniae*, and *Streptococcus pyogenes* (31–46). The majority of characterized Mn uptake systems belong to the NRAMP or ABC transporter families (10, 45). While Mn and Zn importers are known to contribute to disease, their specific roles during infection have been difficult to resolve. This difficulty stems from the ability of these systems to transport or bind noncognate metals *in vitro* and an inability to manipulate Mn and Zn availability within the host (10, 39, 43–51).

S. aureus expresses two metal uptake systems that promote Mn acquisition *in vitro*, the ABC transporter MntABC and the NRAMP homolog MntH (42). In *S. aureus*, MntA and MntB are the ATP binding protein and permease, respectively, while MntC is a solute binding protein. Similar to homologous systems in other species, MntABC and MntH are capable of transporting numerous metals *in vitro*, which has made the physiologically relevant elements transported during *S. aureus* infection difficult to determine (42, 45, 52, 53). Studies using *S. aureus* strain 8325-4 found that loss of MntABC and MntH results in increased sensitivity to the superoxide-generating compound paraquat, and that this mutant exhibits a growth defect in Mn-depleted medium (42). These studies also suggest that *mntH* is constitutively expressed, while *mntABC* expression increases in response to Mn limitation (42). MntC is expressed following intraperitoneal infection, supporting the model that *S. aureus* is Mn limited within the host. Concurrent inactivation of both MntABC and MntH results in decreased bacterial burdens in a staphylococcal skin abscess model of infection, and MntC is currently being considered as part of a multivalent vaccine against *S. aureus* (42, 52). In CP-deficient mice, the increased availability of Mn within *S. aureus* liver abscesses provides a means to determine if the virulence defect of a strain lacking MntABC and MntH is due a reduced ability to acquire Mn or other metals during staphylococcal infection (14).

In this work, we report that MntH and MntABC contribute to infection by enhancing the ability of *S. aureus* to resist Mn starvation imposed by CP. Growth assays utilizing *mnt* mutants and CP variants with altered metal-binding properties demonstrated that MntABC and MntH promote *S. aureus* resistance to Mn starvation. MntABC and MntH promote the retention of superoxide dismutase activity, preventing the accumulation of oxidative stress when starved of Mn by CP. Infection experiments using both wild-type and CP-deficient mice demonstrated that MntABC and MntH promote Mn acquisition during *S. aureus* infection and are critical for systemic staphylococcal disease. Additionally, we report that while the basal level of Mn varies between organs, even in tissues with relatively low Mn abundance, the availability of this metal is further restricted during infection. In total, these results reveal the critical nature of the struggle for Mn during host-pathogen interactions.

MATERIALS AND METHODS

Strains. *S. aureus* strain Newman and derivatives were used for all experiments. The Δ*mntC* and Δ*mntH* deletions were created by amplifying the 5′ and 3′ regions using the indicated primers (Table 1). These fragments were cloned into the pKOR1 knockout vector via site-specific recombination, and the deletions then were created using allelic replacement as previously described (54). To construct vectors for complementation analysis, the *mntC* and *mntH* coding sequence was amplified with the appropriate primer pair (Table 1) and cloned into pOS1 under the control of the P_{lgt} promoter. The sequences of all constructs were confirmed prior to use, and all mutants were hemolytic when plated on sheep blood agar plates. For routine overnight cultures, *S. aureus* strains were grown in 5 ml of tryptic soy broth (TSB) in 15-ml conical tubes at 37°C on a roller drum.

Growth assays. Fifty percent inhibitory concentration (IC_{50}) assays were performed as described previously, with minor modifications (18, 27). Briefly, overnight cultures were back-diluted 1/50 into fresh TSB and grown for 1 h at 37°C. These cultures were then back-diluted 1/100 in 96-well round-bottom plates containing 100 μl of growth media consisting of 38% TSB and 62% calprotectin buffer (CPB) (20 mM Tris, pH 7.5, 100 mM NaCl, 3 mM $CaCl_2$,10 mM β-mercaptoethanol) supplemented with 4 μM $MnCl_2$ and 2 μM $ZnSO_4$. These cultures were incubated with shaking at 37°C, and growth was assessed by measuring the optical density at 600 nm (OD_{600}) at 9 h, which was utilized to calculate the IC_{50}. For complementation experiments, the initial back-dilution was grown for 2 h at 37°C, and 10 μg/ml chloramphenicol was added to all growth media. Purified calprotectin was produced as described previously (18, 27).

Oxidative stress assays. Superoxide sensitivity assays, intracellular superoxide assays, and superoxide dismutase (SOD) activity assays were performed as previously described, with minor modifications (18, 27). For all three assays, bacteria were grown overnight in 5 ml of TSB. The next morning, these cultures were back-diluted 1/100 into round-bottom 96-well trays containing 38% brain heart infusion supplemented with 0.5% glucose and 62% CPB. These cultures were then grown at 37°C with shaking at 180 rpm. For superoxide sensitivity assays, the growth medium was supplemented with various concentrations of the superoxide-generating compound paraquat, 4 μM $MnCl_2$, and 2 μM $ZnSO_4$. Growth was assessed at 7 h by measuring the optical density at 600 nm (OD_{600}). For intracellular superoxide assays, bacteria were grown for 7 h in media with or without 4 μM $MnCl_2$ and 2 μM $ZnSO_4$, as indicated. Following growth, the bacteria were incubated with dihydroethidium for 35 min at 37°C, harvested, and assessed for ethidium bromide (EtBr) DNA fluorescence, as previously described (18, 27). For SOD activity assays, bacteria were grown to mid-exponential phase in media supplemented with 4 μM $MnCl_2$, 2 μM $ZnSO_4$, and 1 mM paraquat and then harvested and lysed via bead beating in 25 mM Tris buffer, pH 8.0, as previously described (18, 27). SOD activity was assessed via water-soluble tetrazolium salt assay (Sigma-Aldrich, St. Louis, MO), and total protein was determined via bicinchoninic acid (BCA) assay (Pierce Thermo-Fisher, Rockford, IL).

Expression analysis. To assess the expression of *mntH* and *mntA* under conditions of Zn, Mn, or Fe limitation, *S. aureus* was grown overnight in TSB and then subcultured 1/100 into Chelex-treated RPMI plus 1% Casamino Acids supplemented with 1 mM $MgCl_2$, 100 μM $CaCl_2$, 25 μM $ZnSO_4$, 25 μM $MnCl_2$, or 1 μM $FeSO_4$. To create Zn-, Mn-, or Fe-deficient media, salts containing these metals were omitted from the growth media as indicated. Bacterial cultures, 5 ml in a 15-ml conical tube, were grown at 37°C with rotation until mid-exponential phase. Upon reaching mid-exponential phase, an equal volume of ice-cold 1:1 acetone-ethanol was added to the cultures, which were then frozen at −80°C until RNA could be extracted. To assess the impact of CP treatment on *mntH* and *mntA*, *S. aureus* was back-diluted 1/50 from an overnight culture into 5 ml of TSB and incubated for 1 h at 37°C with rotation. This culture was then used to inoculate 100 μl of culture media (38% TSB and 62% CPB supplemented with 1 μM $MnCl_2$, 1 μM $ZnSO_4$, and various concentrations of calprotectin) in a 96-well round-bottom plate. The cultures were grown at 37°C with shaking until reaching mid-exponential phase, when the samples were harvested and preserved in acetone-ethanol at −80°C. RNA was extracted and cDNA was created, as previously described (55, 56). Expression of *mntA* and *mntH* was assessed by quantitative reverse transcription-PCR (qRT-PCR) using the indicated primer sets (Table 1), and 16S RNA was used as a normalizing control.

Animal infections. All animal experiments were approved by the Vanderbilt Institutional Animal Care and Use Committee. For all experiments, mice were infected retro-orbitally with approximately 1×10^7 CFU in 100 μl of sterile phosphate-buffered saline, as previously described (14, 18). Following injection, the infection was allowed to proceed for 96 h and the mice were then sacrificed. Livers and kidneys were removed following autopsy and subjected to evaluation of bacterial burden, elemental analysis using inductively coupled plasma mass spectrometry (ICP-MS), and protein distribution determination using matrix-assisted laser desorption ionization imaging mass spectrometry (MALDI IMS). To determine bacterial load, organs were homogenized and dilutions were plated to enumerate CFU. For imaging mass spectrometry-based analysis, organs were flash-frozen in a slurry of dry ice and technical-grade hexanes (Sigma-Aldrich, St. Louis, MO) and then stored at −80°C.

Quantitative total tissue elemental analysis. Quantitative analysis was performed on a Thermo Element 2 high-resolution sector field inductively coupled plasma mass spectrometer (Thermo Fisher Scientific, Bremen, Germany). Following organ harvest, the samples were placed in Optima-grade nitric acid and sulfuric acid (Fisher Scientific, Pittsburgh, PA) and then heated to promote digestion. After digestion, the samples were diluted using Milli-Q ultrapure water (Millipore, Billerica, MA). The introduction of diluted acid-digested samples was conducted by an electrospray ionization (ESI) autosampler (Elemental Scientific, Omaha, NE) via a sample probe (0.50-mm inner diameter) and sample capillary in self-aspiration mode. The sample capillary was directly connected to a PFA MicroFlow nebulizer (Elemental Scientific, Omaha, NE), followed by a double-channel spray chamber (at room temperature). The fine sample aerosol formed in the spray chamber was then transported by argon gas to hot plasma for vaporization, atomization, and ionization. All analyte ions then were filtered and separated by magnetic sector and electric sector for the selected element isotopes, which were detected by SEM. The operation parameters of ICP-MS are listed in Table 2.

TABLE 2 ICP-MS parameters for quantitative elemental analysis

Parameter	Value
RF power (W)	1,250
Cool gas (liter min^{-1})	16.00
Auxiliary gas (liter min^{-1})	0.8
Sample gas (liter min^{-1})	0.97
Resolution mode	Medium (4,300)
Isotopes measured	^{25}Mg, ^{31}P, ^{44}Ca, ^{55}Mn, ^{56}Fe, ^{63}Cu, ^{66}Zn
Runs (no.)	10
Passes (no.)	1
Samples per peak (no.)	20

Preparation of tissue sections for MALDI IMS, LA-ICP-MS, and histological examination. For MALDI IMS, histological examination, and laser ablation inductively coupled plasma mass spectrometry (LA-ICP-MS), kidney tissue was sectioned at −20°C using a Leica CM3050S cryostat (Leica Microsystems, Bannockburn, IL). Serial sections were mounted for MALDI IMS, histological analysis, and LA-ICP-MS. Sections for MALDI IMS were 10 μm thick and were thaw mounted onto chilled indium-tin oxide (ITO)-coated glass slides (Delta Technologies, Loveland, CO). Sections for histological analysis were 10 μm thick and were thaw mounted onto glass microscope slides. Sections for LA-ICP-MS were 30 μm thick and were mounted to chilled nitric acid-washed polylysine-coated vinyl slides. Samples for each type of analysis were then further processed as described below.

MALDI IMS. Serial sections for MALDI IMS were washed to remove excess lipids and salts. Slides were sequentially washed in 70% ethanol for 30 s, 100% ethanol for 30 s, Carnoy's fluid (6:3:1 ethanol-chloroform-acetic acid) for 2 min, 100% ethanol for 30 s, 0.2% trifluoracetic acid (TFA) for 30 s, and 100% ethanol for 30 s. Slides were allowed to dry before matrix was applied. For the matrix, a 5 mg/ml solution of sinapinic acid matrix was prepared in 60% acetonitrile with 0.1% TFA and sonicated for 5 min to ensure that the matrix was completely dissolved. Matrix was applied using a TM-Sprayer (HTX Imaging, Carrboro, NC) heated to 90°C in 8 passes at a rate of 1,050 mm/min with a 2-mm spacing. The spray pattern was spatially alternated at a 90° angle and offset by 1 mm to ensure uniform sample coverage. After matrix application, samples were rehydrated at 85°C in an oven (Oven Series 1297; Thermolyne, Dubuque, IA). Samples were fixed to the lid of a petri dish using conductive tape and preheated in the oven for 2 min. Following this, 1 ml of water and 100 μl of acetic acid were pipetted onto filter paper in the petri dish bottom. The petri dish was reassembled to form a rehydration chamber and was heated at 85°C for an additional 3.5 min. The rehydrated slide was allowed to dry at room temperature before analysis. Trifluoroacetic acid (TFA) and sinapinic acid were purchased from Sigma-Aldrich (St. Louis, MO). High-performance liquid chromatography (HPLC)-grade acetonitrile, ethanol, chloroform, and glacial acetic acid and technical-grade hexanes were purchased from Fisher Scientific (Pittsburgh, PA).

Following rehydration, the tissue was analyzed using a Bruker Autoflex speed tandem time-of-flight (TOF/TOF) mass spectrometer (Bruker Daltonics, Billerica, MA) equipped with a Gaussian beam profile laser (Nd:YAG; 355 nm) in linear positive-ion mode at 75-μm spatial resolu-

TABLE 3 Experimental parameters for LA-ICP-MS

Assay and parameter[a]	Value
Laser ablation system	
Wavelength of Nd:YAG laser (nm)	200
Laser spot size (μm)	100
Distance between lines (μm)	10
Laser energy (%)	50
Laser shot frequency (Hz)	20
Scan rate (μm/s)	20
ICP-MS	
RF power (W)	1,250
Cool gas (Ar) (liters min^{-1})	16.00
Auxiliary gas (Ar) (liters min^{-1})	0.8
Sample gas (Ar) (liters min^{-1})	1.0
Resolution mode	Medium (4,300)
Isotopes measured	^{44}Ca, ^{55}Mn, ^{66}Zn
Samples per peak (no.)	20

[a] The laser ablation system used was LSX-213, CETAC. For ICP-MS, an Element 2 device (Thermo Fisher Scientific) was used.

tion. One hundred laser shots were collected at each position in a random walk pattern in 25-shot step increments, with a laser repetition rate of 1,000 Hz. Extraction and acceleration voltages were 19.5 and 18.0 kV, respectively, with a delayed extraction time of 340 ns and a lens voltage of 7.5 kV. The measured mass range was from *m/z* 3,000 to 30,000, with a deflection mass of 3,000. Images were viewed using Fleximaging 3.0 software (Bruker Daltonics) and were normalized to total ion current. Ion density maps were extracted, and scaling, relative to total ion current, was constant for each ion of interest.

Histology. Serial sections collected for histological analysis were hematoxylin and eosin (H&E) stained. Stained slides were scanned using a MIRAX scan slide scanner (Carl Zeiss MicroImaging, Gottingen, Germany) in manual bright-field mode. Optical images were generated from the scans using MIRAX viewer, version 1.11.22.0 (Carl Zeiss MicroImaging).

Elemental imaging by LA-ICP-MS. All elemental imaging measurements were performed by a laser ablation system (LA; LSX-213; CETAC, Omaha, NE) coupled with a high-resolution sector field inductively coupled plasma mass spectrometer (ICP-MS; Element 2; Thermo Fisher Scientific, Bremen, Germany). Slide-mounted slices of kidney tissue were placed in a sealed ablation cell and ablated in multiline mode (line by line) with a focused Nd:YAG laser beam that operated at a quadrupled wavelength of 213 nm, energy of 50%, laser shot frequency of 20 Hz, and laser spot size of 100 μm. Helium gas was used as the cell gas during ablation for better sample transport efficiency. The ablated sample particles were transported by He from the ablation cell and then mixed with argon gas before online introduction into the ICP-MS for element intensity detection of the following ions: $^{44}Ca^+$, $^{55}Mn^+$, and $^{66}Zn^+$. The operational parameters for the laser ablation system and ICP-MS are listed in Table 3.

Statistical analysis. Statistical analysis was performed using Graph Pad Prism, version 5.0, and the indicated statistical test.

RESULTS

Mn sequestration by calprotectin increases the expression of *S. aureus* Mn uptake systems. Two of the metal uptake systems expressed by *S. aureus*, MntABC (NWMN_0601-NWMN_0603) and MntH (NWMN_0971), have been characterized as Mn transporters (42). As an initial step in evaluating whether these systems contribute to resisting the effects of host-imposed Mn and Zn limitation, changes in *mntA* and *mntH* transcript levels in response to CP-induced metal starvation *in vitro* were assessed. In response to CP, the level of *mntA* and *mntH* transcripts increased (Fig. 1A). As CP sequesters both Mn and Zn, it is possible that the availability of only one or both of these metals is influencing the expression of MntABC and MntH. To define which metals affect the expression of the Mnt systems, *S. aureus* was grown in metal-defined media lacking Mn or Zn. The expression of *mntA* and *mntH* was also assessed in Fe-depleted media, as Fe has been shown to interact with orthologs of these systems (45). Using specific metal-depleted media, *mntA* transcript levels increased only in the absence of Mn (Fig. 1B) (42). This supports a model whereby changes in *mntA* transcript following CP exposure are due to decreased Mn availability and not decreased Zn availability. Surprisingly, *mntH* transcript levels increased only when Mn, Zn, and Fe all were omitted from the media (Fig. 1B). This suggests that the increased *mntH* transcript levels in the presence of CP are due to simultaneous reductions in the levels of both Mn and Zn.

Expression of MntABC and MntH specifically promotes staphylococcal growth in response to host-imposed Mn starvation. To determine whether MntABC and MntH enable *S. aureus* to compete with CP for nutrient Mn and/or Zn, we first created strains inactivated for *mntC* or *mntH* alone or in combination (Δ*mntH*, Δ*mntC*, and Δ*mntC* Δ*mntH* mutants). While the Δ*mntC* Δ*mntH* mutant does not have a growth defect in TSB, this strain grows more poorly in CP medium (38% TSB and 62% calprotectin buffer [CPB]), presumably due to the reduced metal availability under this condition (data not shown). When CP medium was supplemented with 4 μM $MnCl_2$, the Δ*mntC* Δ*mntH* mutant grew as well as wild-type *S. aureus* (see Fig. S1 in the supplemental material). To assess the role of MntABC and MntH in promoting *S. aureus* growth when this organism is starved of Mn and Zn by the host, the concentration of CP that results in a 50% inhibition of growth (IC_{50}) was determined for Δ*mntH*, Δ*mntC*, and Δ*mntC* Δ*mntH* mutants. While the Δ*mntH* and

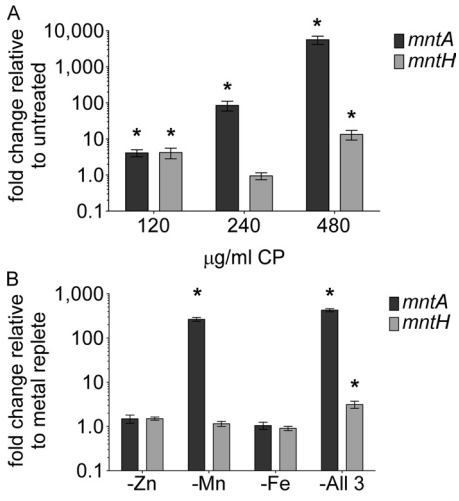

FIG 1 Calprotectin-induced metal starvation increases the expression of MntABC and MntH. (A) *S. aureus* was grown in the presence of increasing concentrations of CP, and transcript levels of *mntA* and *mntH* were assessed by qRT-PCR. Expression was compared to that of bacteria grown in untreated media. (B) Transcript levels of *mntA* and *mntH* were assessed by qRT-PCR following growth in metal-defined media with Zn, Mn, Fe, or all three metals omitted. Expression was compared to that of metal-replete media. *, $P < 0.05$ via one-way analysis of variance (ANOVA) with Dunnett's posttest versus untreated media or metal-replete media. Error bars represent standard errors of the means (SEM) ($n = 5$).

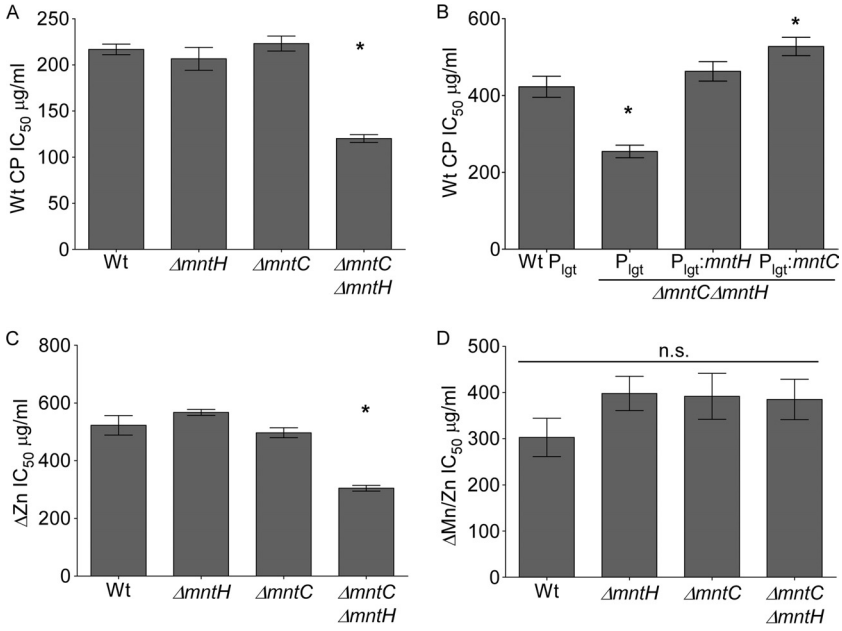

FIG 2 MntABC and MntH promote *S. aureus* growth when starved of Mn by calprotectin. (A, C, and D) Wild-type *S. aureus* or Δ*mntH*, Δ*mntC*, or Δ*mntC* Δ*mntH* mutant strains were grown in the presence of increasing concentrations of wild-type CP (A), the ΔZn site mutant (C), or the ΔMn/Zn site mutant (D), and the IC_{50} was determined. (B) Wild-type *S. aureus* pOS1P_{lgt} and the Δ*mntC* Δ*mntH* pOS1P_{lgt}, Δ*mntC* Δ*mntH* pOS1P_{lgt}::*mntH*, and Δ*mntC* Δ*mntH* P_{lgt}::*mntC* mutants were grown in the presence of increasing concentrations of wild-type CP, and the IC_{50} was determined. *, $P < 0.05$ via one-way ANOVA with Dunnett's posttest compared to results for wild-type *S. aureus*. Error bars represent SEM ($n = 3$ to 6).

Δ*mntC* mutants were not more sensitive to CP, the Δ*mntC* Δ*mntH* mutant was twice as sensitive to CP as wild-type *S. aureus* (Fig. 2A; also see Fig. S2A to D in the supplemental material). Expression of either *mntC* or *mntH in trans* reversed the increased sensitivity of the Δ*mntC* Δ*mntH* mutant to CP, indicating that the growth defect of the Δ*mntC* Δ*mntH* mutant is not due to secondary mutations (Fig. 2B). In total, these results demonstrate that both MntABC and MntH contribute to resisting CP-dependent metal limitation.

The increased sensitivity to metal starvation highlights the important role of metal importers in resisting the effects of CP; however, it does not indicate whether MntABC and MntH protect *S. aureus* from Mn limitation, Zn limitation, or both. The creation of CP variants with altered metal binding properties circumvents this technical challenge (27). Specifically, utilization of variants that lack the Zn site (ΔZn mutant) or the Mn/Zn site (ΔMn/Zn mutant) allow the contributions of the MntABC and MntH systems to resisting CP-mediated Mn and/or Zn sequestration to be evaluated (27). When grown in the presence of the ΔZn variant that retains the ability to bind a single Zn or Mn ion, the IC_{50} of the Δ*mntC* Δ*mntH* mutant was reduced compared to that of wild-type *S. aureus* (Fig. 2C). However, when the Δ*mntC* Δ*mntH* mutant was grown in the presence of the ΔMn/Zn variant that binds Zn but not Mn, the IC_{50} of the Δ*mntC* Δ*mntH* mutant was similar to that of the wild type (Fig. 2D). These results indicate that expression of MntH and MntABC protects *S. aureus* from CP-imposed Mn sequestration.

MntABC and MntH promote the retention of superoxide dismutase activity. In addition to inhibiting essential bacterial processes, CP also inhibits Mn-dependent superoxide dismutase (SOD) activity that, while dispensable for growth, protects against the oxidative burst of the host (18, 27, 30). To determine if expression of Mn importers promotes retention of SOD activity when starved of Mn by the host, the Δ*mntH*, Δ*mntC*, and Δ*mntC* Δ*mntH* mutants were assessed for sensitivity to the superoxide-generating compound paraquat in the presence of CP. CP-imposed Mn starvation rendered the Δ*mntC* Δ*mntH* mutant, but not the Δ*mntH* or Δ*mntC* mutant, more sensitive to the toxic effects of paraquat than wild-type *S. aureus* (Fig. 3A; also see Fig. S3A to E in the supplemental material). Recent work has revealed that paraquat toxicity is not due solely to the generation of oxidative stress, although the primary mechanism of toxicity in SOD-deficient strains is superoxide production (57–60). In order to directly test whether bacterial defenses against oxidative stress are impaired in the *mnt* mutants, SOD activity in the Δ*mntH*, Δ*mntC*, and Δ*mntC* Δ*mntH* mutants was assessed following CP treatment. Concomitant inactivation of both MntC and MntH ablated *S. aureus* SOD activity in the presence of CP (Fig. 3B). In Mn-supplemented medium, the Δ*mntC* Δ*mntH* mutant exhibited a 3-fold reduction in SOD activity at 240 μg/ml CP, the lowest concentration of CP tested. Increasing the concentration of CP further reduced the SOD activity of the Δ*mntC* Δ*mntH* mutant (Fig. 3B). To achieve a 3-fold reduction in SOD activity in wild-type bacteria, 960 μg/ml of CP was needed under similar growth conditions, highlighting the importance of MntABC and MntH for maximal SOD activity (Fig. 3B). In addition to the Δ*mntC* Δ*mntH* mutant, Δ*mntC* exhibited reduced SOD activity relative to that of wild-type *S. aureus* when treated with CP (Fig. 3B). To assess if the *mnt* mutants experience enhanced oxidative stress following CP treatment, intracellular superoxide levels were assessed. Consistent with the reduced SOD activity in Mn-supplemented growth media, Δ*mntC* Δ*mntH* and Δ*mntC* mutants displayed elevated intracellular superoxide levels following CP treatment when grown in the same conditions (see Fig. S3F in the supplemental material). All of

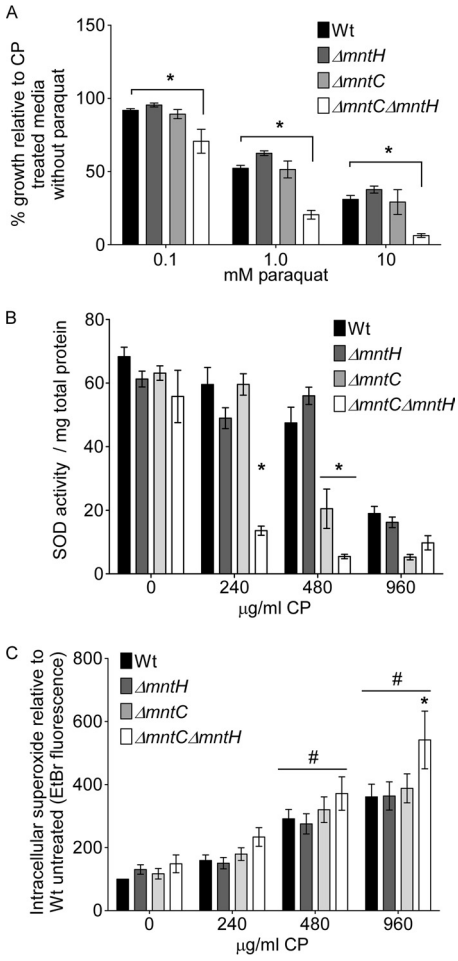

FIG 3 Loss of MntABC and MntH results in reduced elaboration of oxidative stress defenses in the presence of calprotectin. (A) Impact of CP on the superoxide sensitivity of *mnt* mutants. Wild-type *S. aureus* and Δ*mntH*, Δ*mntC*, and Δ*mntC* Δ*mntH* mutants were grown in the presence of medium supplemented with 480 μg/ml wild-type CP, 4 μM $MnCl_2$, 2 μM Zn SO_4, and various concentrations of paraquat. *, $P < 0.05$ via two-way ANOVA with Bonferroni's posttest. Error bars indicate SEM ($n = 3$). (B) Wild-type *S. aureus* and Δ*mntH*, Δ*mntC*, and Δ*mntC* Δ*mntH* mutants were grown in Mn-supplemented media in the presence of wild-type CP and 1 mM paraquat, and superoxide dismutase activity was assessed. *, $P < 0.05$ compared to the wild type via two-way ANOVA with Bonferroni's posttest. Error bars indicate SEM ($n = 6$ to 7). (C) Intracellular superoxide levels of wild-type *S. aureus* and Δ*mntH*, Δ*mntC*, and Δ*mntC* Δ*mntH* mutants following CP treatment. Bacteria were grown in Mn-supplemented media treated with various concentrations of wild-type CP, and intracellular superoxide levels were determined by dihydroethidium assay. *, $P < 0.05$ via two-way ANOVA with Bonferroni's posttest relative to the wild type treated with the same concentration of CP. #, $P < 0.05$ relative to untreated wild type via two-way ANOVA with Bonferroni's posttest. Error bars represent SEM ($n = 5$).

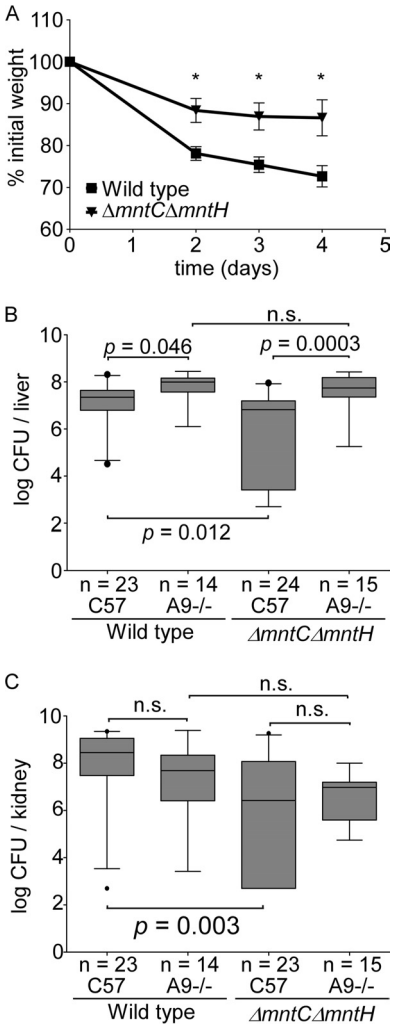

FIG 4 MntABC and MntH are necessary for invasive *S. aureus* disease and promote Mn acquisition during infection. Nine-week-old C57BL/6 (C57) or C57BL/6 S100A9$^{-/-}$ (A9$^{-/-}$) mice were infected with either wild-type *S. aureus* or the Δ*mntC* Δ*mntH* mutant. We assessed weight loss as a percentage of initial weight (A), and bacterial burdens in the liver (B) and the kidneys (C) were assessed. The data presented are results from three independent experiments. For panel A, an asterisk indicates a *P* value of less than 0.05 via two-way ANOVA corrected for repeated measurements with Bonferroni's posttest. Error bars represent SEM ($n = 23$ [wild type] or 24 [Δ*mntC* Δ*mntH* mutant]). (B and C) Statistical significance was determined by Mann-Whitney test, and significance is indicated for each comparison where *P* is less than 0.05. The bar represents the median value, boxes the interquartile range, and whiskers the 5th to 95th percentile; circles indicate data points falling outside this range.

the strains accumulated higher levels of intracellular superoxide upon CP treatment when the growth medium was not supplemented with Mn (Fig. 3C). However, oxidant levels in the Δ*mntC* Δ*mntH* mutant were significantly higher than those in wild-type bacteria (Fig. 3C). These results reveal the critical contribution of Mn importers to maintaining SOD activity.

Expression of Mn importers is necessary to combat host-imposed Mn starvation during infection. Previous studies have revealed that MntABC and MntH contribute modestly to *S. aureus* disease in a skin model of infection (42). To assess the contribution of the MntABC and MntH importers to resisting host-imposed Mn sequestration during systemic infection, wild-type C57BL/6 mice or CP-deficient mice (C57BL/6 S100A9$^{-/-}$) were infected with either wild-type *S. aureus* or the Δ*mntC* Δ*mntH* mutant. During the course of infection, C57BL/6 mice infected with the Δ*mntC* Δ*mntH* mutant were more active and lost significantly less weight than wild-type mice infected with wild-type *S. aureus* (Fig. 4A and data not shown).

After 4 days of infection, livers and kidneys were harvested and CFU were enumerated following organ homogenization. Wild-type C57BL/6 mice infected with the Δ*mntC* Δ*mntH* mutant had

significantly lower bacterial burdens in the liver and kidneys than wild-type mice infected with wild-type *S. aureus*, suggesting a critical role for staphylococcal importers during the development of invasive disease (Fig. 4B and C). MALDI IMS demonstrated that CP is recruited at levels similar to those of abscesses formed in response to infection with wild-type *S. aureus* or the Δ*mntC* Δ*mntH* mutant (see Fig. S4 in the supplemental material). Consistent with previous results, the livers of CP-deficient mice infected with wild-type *S. aureus* had increased bacterial burdens compared to wild-type C57BL/6 mice (Fig. 4B) (14, 18). CP-deficient mice infected with the Δ*mntC* Δ*mntH* mutant had significantly higher bacterial burdens than wild-type mice that had been infected with the Δ*mntC* Δ*mntH* mutant (Fig. 4B). Loss of CP-mediated Mn sequestration reversed the virulence defect observed with wild-type mice and allowed the Δ*mntC* Δ*mntH* mutant to infect livers as well as wild-type bacteria (Fig. 4B). These results demonstrate that MntABC and MntH compete with CP to enable Mn acquisition and full virulence during systemic infection.

In wild-type mice, the Δ*mntC* Δ*mntH* mutant had a virulence defect in the kidneys compared to wild-type *S. aureus* (Fig. 4C). This defect suggests that during infection, the kidney is also a Mn-depleted environment. However, unlike in the liver, the kidneys of CP-deficient mice infected with wild-type *S. aureus* do not have increased bacterial burdens (Fig. 4C). When infected with the Δ*mntC* Δ*mntH* mutant, the kidneys of CP-deficient mice had a modest but not significant increase in bacterial burdens compared to wild-type mice (Fig. 4C). The reduced bacterial burdens in the kidneys following infection with the Δ*mntC* Δ*mntH* mutant suggest that similar to the liver, this organ is Mn limited. The absence of a phenotype in the kidney of CP-deficient mice infected with wild-type *S. aureus* or the Δ*mntC* Δ*mntH* mutant suggests the presence of CP-independent mechanisms for Mn sequestration in this organ. In total, these results demonstrate that the expression of Mn importers is critical for the development of invasive staphylococcal disease. Furthermore, the similar bacterial burdens in the livers of CP-deficient mice infected with either wild-type bacteria or the Δ*mntC* Δ*mntH* mutant highlights the critical role these systems play in acquiring Mn and the importance of restricting the availability of this metal during infection.

Vertebrates possess multiple mechanisms for sequestering Mn from the *S. aureus* abscess. The distinct phenotypes in the livers and kidneys of CP-deficient mice suggest that the availability of metals within these two organs is different. Total metal analysis of kidneys and liver indicated that uninfected kidneys contain half as much Mn and Zn per gram of tissue as liver (Fig. 5 and Table 4). Upon infection, the total Mn content in the kidneys was unaffected, whereas Mn levels decreased in the liver. Conversely, Zn levels remained the same in the kidneys following infection but increased in the livers of infected animals. Although the kidneys appear to be Mn limited, the similar bacterial burdens in the kidneys of wild-type and CP-deficient mice suggest that CP does not contribute substantially to Mn sequestration in this organ (14). To address this possibility, IMS was employed to image metal and protein levels in infected organs (14, 61–66). Imaging LA-ICP-MS was used to examine metal distribution in the kidneys of wild-type C57BL/6 and CP-deficient mice infected with *S. aureus*. As calcium has been previously shown to accumulate in staphylococcal abscesses, the signal for this element was used to align LA-ICP-MS images with the H&E-stained sections (14). This analysis demonstrated that, despite the relatively low bulk level of Mn and Zn in

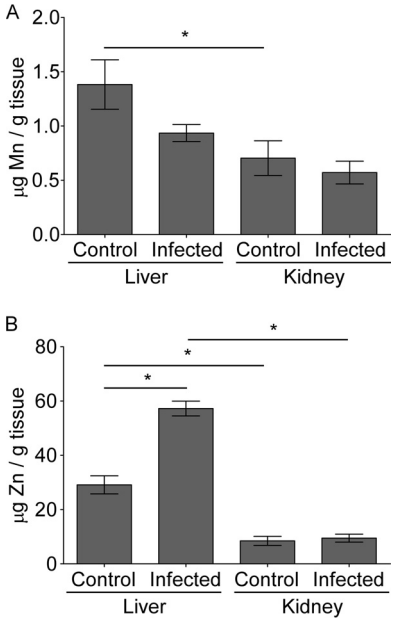

FIG 5 Total tissue Mn and Zn levels vary by organ and are influenced by infection. To assess the impact of infection on bulk metal availability, 9-week-old C57BL/6 mice were infected with wild-type *S. aureus* or mock infected with PBS. Following 4 days of infection, livers and kidneys were harvested, and total Mn (A) and Zn (B) content was assessed by inductively coupled plasma mass spectrometry. *, $P = 0.05$ via one-way ANOVA with Bonferroni's posttest. Error bars indicate SEM ($n = 5$ to 10).

the kidney, abscesses in wild-type kidneys are more restricted for both of these metals than the surrounding tissue (Fig. 6; also see Fig. S5 in the supplemental material). These images also suggest that the tissues surrounding the abscess have elevated levels of Zn. MALDI IMS analysis of infected kidneys found that S100A8 and S100A9 localize to sites of Mn and Zn restriction in wild-type mice during infection (Fig. 6). Consistent with the dependency of S100A8 on S100A9 for stability *in vivo*, neither subunit is detectable in the kidneys of infected C57BL/6 S100A9$^{-/-}$ mice (Fig. 6) (67). In contrast to what is observed in liver abscesses of CP-deficient animals (14), the kidney abscesses of both wild-type and CP-deficient mice have lower levels of Mn and Zn than the surrounding tissue (Fig. 6; also see Fig. S5 in the supplemental material). These results support the proposal that vertebrates restrict access to Mn and Zn during infection and suggest that CP-independent mechanisms for restricting Mn exist within the kidney.

DISCUSSION

Restricting the availability of the essential elements Mn and Zn is a powerful strategy utilized by the host to control invading pathogens. Despite this restriction, *S. aureus* and other pathogens remain capable of causing disease, suggesting that they elaborate specific mechanisms for overcoming Mn and Zn limitation. Studies using engineered variants of CP with altered metal binding properties revealed that the expression of MntABC and MntH both increases bacterial growth and promotes elaboration of a more robust defense against oxidative stress when metal starved by the host. The use of CP-deficient mice revealed that the virulence defect of the Δ*mntC* Δ*mntH* mutant is specifically due to an inability to acquire Mn during infection. Further emphasizing the

TABLE 4 Analysis of tissue metal levels

Element	Metal level (μg/g tissue) in[a]:			
	Liver uninfected	Liver infected	Kidney uninfected	Kidney infected
Magnesium	240.13 ± 37.62	294.41 ± 7.45	94.50 ± 18.76	99.61 ± 14.62
Phosphorous	3,240.38 ± 466.29	3,855.39 ± 118.25	1,658.38 ± 369.50	1,656.70 ± 304.79
Calcium	48.78 ± 7.98	98.51 ± 4.67	29.60 ± 5.84	45.21 ± 6.73
Manganese	1.38 ± 0.23	0.94 ± 0.08	0.70 ± 0.16	0.57 ± 0.10
Iron	192.85 ± 37.48	252.64 ± 7.80	50.64 ± 10.18	52.44 ± 8.32
Copper	4.39 ± 0.63	6.13 ± 0.36	2.05 ± 0.41	1.76 ± 0.28
Zinc	29.12 ± 3.33	57.25 ± 2.73	8.47 ± 1.68	9.48 ± 1.46

[a] Data are results ± SEM (n = 5 to 10).

importance of Mn sequestration to host defense is the observation that a Δ*mntC* Δ*mntH* mutant has bacterial burdens comparable to those of wild-type *S. aureus* in the livers of CP-deficient mice. These studies reveal the importance of the struggle for nutrient metals between host and pathogen and how altering this balance can determine the outcome of infection.

Orthologs of the *S. aureus* MntABC and MntH systems are widespread among bacterial pathogens and contribute to the pathogenesis of *Brucella abortus*, *Yersinia pestis*, *Streptococcus pneumoniae*, and *Streptococcus pyogenes* (38–46). However, with many pathogens, technical challenges associated with determining the relevant metal transported *in vivo* have made elucidating the specific contributions of MntABC and MntH orthologs to infection difficult (10, 45). Transport studies have been the primary means of assessing the metal specificity of NRAMP homologs, and these studies often suggest an ability to transport multiple metals (45). For ABC-type transporters, binding and structural studies utilizing the solute binding protein have been the primary means of elucidating metal specificity (45). Analysis of PsaABC from *S. pneumoniae* revealed that the solute binding protein is capable of binding Zn (47, 51). Despite this observation, it has become apparent that the binding of Zn poisons the PsaABC system by preventing *S. pneumoniae* from acquiring Mn, highlighting the hazards of relying on binding studies (51). Due to the difficulty in manipulating *in vivo* metal levels, availability and transporter affinity have been used to argue that virulence defects

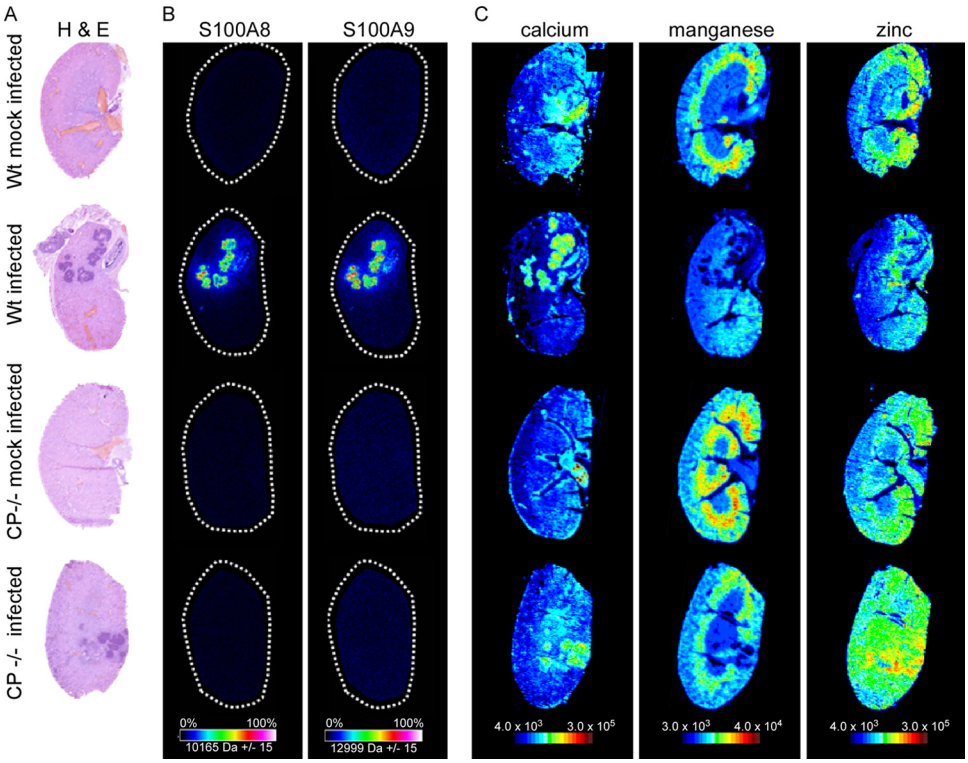

FIG 6 In tissues with relatively low basal levels of Mn and Zn, access to these metals is further restricted during infection. To assess the distribution of Mn and Zn within the kidney during infection, C57BL/6 or CP-deficient (S100A9$^{-/-}$) mice were infected with wild-type *S. aureus* or mock infected with PBS. Following 4 days of infection, the tissues were harvested and analyzed by H&E staining (A), MALDI IMS for CP distribution (B), and LA-ICP-MS for calcium, manganese, and zinc distribution (C). (B) Scale represents percent maximal ion intensity. To assess the distribution of S100A8, a mass of 10,165 Da was mapped. For S100A9, a mass of 12,999 Da was mapped, which corresponds to S100A9 in complex with a sodium ion. (C) Scale represents absolute ion intensity for the indicated metal. Images are representative of two independent experiments.

associated with the loss of MntABC and MntH orthologs in other bacteria are associated with defects in Mn acquisition during infection (10, 45). The observation that *S. aureus* MntABC and MntH promote Mn acquisition during infection lends further support to these hypotheses.

Despite the fact that pathogens express dedicated metal uptake systems, these organisms still experience metal starvation during infection. This idea is supported by the increased bacterial and fungal burdens in CP-deficient mice that have a defect in Mn and Zn sequestration (14, 18, 20–22). Further supporting this conclusion is the observation that during infection, the host inhibits staphylococcal superoxide dismutase activity (18). The ability of *S. aureus* and other pathogens to cause devastating disease suggests that these organisms have specific mechanisms that enable them to adapt to host-imposed Mn and Zn starvation. Continued elucidation of the bacterial adaptations that facilitate survival in the metal-depleted environment created by vertebrates has the potential to identify new targets for therapeutic intervention.

The important and multifaceted contributions of metals to the outcome of infection are becoming increasingly apparent. While metals such as Fe and Mn are kept away from bacteria to weaken these invading pathogens, the host appears to leverage the antimicrobial properties of Cu to increase the killing power of phagocytes (10, 18, 27, 68–72). The complexity of the relationship between metals and infection is emphasized by the dual roles of Zn, which is both restricted to control bacterial growth and harnessed for its toxicity (10, 14, 51). The role of metals during infection is further complicated by their need for proper host development and function. Zn is a prime example of this, in that it is removed from the staphylococcal abscess to starve invading pathogens, yet it is required for proper immune development and function (73). Total analysis of tissue metal levels via ICP-MS revealed that, compared to the liver, the kidney is a relatively Mn- and Zn-depleted environment. Further analysis revealed that despite having relatively low basal levels of these metals during infection, access to Mn and Zn becomes even further restricted within staphylococcal kidney abscesses. Surprisingly, while CP is required for Mn sequestration in the liver during infection, kidney abscesses in CP-deficient mice were Mn restricted compared to the surrounding tissues (14). These data suggest that vertebrates possess CP-independent mechanisms for removing Mn from the kidney during infection (14). At this point, there are no clues to the identity of these additional Mn binding proteins.

Bacterial pathogens are a significant threat to human health, and the continued emergence of antimicrobial resistance has only amplified this danger. The results presented here provide new insights into the mechanisms utilized by bacteria to acquire essential nutrients within the host and the extent to which the host restricts metal availability during infection. The continued elucidation of nutrient availability and the mechanisms utilized by pathogens to resist host-imposed starvation will provide a foundation for the development of novel therapeutics.

ACKNOWLEDGMENTS

We thank the members of the Skaar laboratory for critical reading of the manuscript.

This work was supported by R56 AI091771 and R01 AI101171 to E.P.S. and W.J.C. T.K.F. was supported by postdoctoral fellowships from the American Heart Association and the NIH (F32 AI100480). J.L.M. was supported by the Vanderbilt Chemical Biology Interface training program (T32 GM008320). This work was also supported in part by NIH/NCRR (1P41RR031461), awarded to R.M.C. M.I.H. was supported by an International Student Research Fellowship from the Howard Hughes Medical Institute and by a Public Health Service award for the Vanderbilt Medical-Scientist Training Program (T32 GM07347). A.J.F. was supported by an NIH postdoctoral fellowship (F32 AI098380).

REFERENCES

1. **Wertheim HF, Vos MC, Ott A, van Belkum A, Voss A, Kluytmans JA, van Keulen PH, Vandenbroucke-Grauls CM, Meester MH, Verbrugh HA.** 2004. Risk and outcome of nosocomial *Staphylococcus aureus* bacteraemia in nasal carriers versus non-carriers. Lancet **364:**703–705.
2. **Lowy FD.** 1998. *Staphylococcus aureus* infections. N. Engl. J. Med. **339:**520–532.
3. **Fridkin SK, Hageman JC, Morrison M, Sanza LT, Como-Sabetti K, Jernigan JA, Harriman K, Harrison LH, Lynfield R, Farley MM.** 2005. Methicillin-resistant *Staphylococcus aureus* disease in three communities. N. Engl. J. Med. **352:**1436–1444.
4. **Grundmann H, Aires-de-Sousa M, Boyce J, Tiemersma E.** 2006. Emergence and resurgence of meticillin-resistant *Staphylococcus aureus* as a public-health threat. Lancet **368:**874–885.
5. **Rybak MJ, Akins RL.** 2001. Emergence of methicillin-resistant *Staphylococcus aureus* with intermediate glycopeptide resistance: clinical significance and treatment options. Drugs **61:**1–7.
6. **Said-Salim B, Mathema B, Kreiswirth BN.** 2003. Community-acquired methicillin-resistant *Staphylococcus aureus*: an emerging pathogen. Infect. Control Hosp. Epidemiol. **24:**451–455.
7. **Weigel LM, Clewell DB, Gill SR, Clark NC, McDougal LK, Flannagan SE, Kolonay JF, Shetty J, Killgore GE, Tenover FC.** 2003. Genetic analysis of a high-level vancomycin-resistant isolate of *Staphylococcus aureus*. Science **302:**1569–1571.
8. **Klevens RM, Morrison MA, Nadle J, Petit S, Gershman K, Ray S, Harrison LH, Lynfield R, Dumyati G, Townes JM, Craig AS, Zell ER, Fosheim GE, McDougal LK, Carey RB, Fridkin SK.** 2007. Invasive methicillin-resistant *Staphylococcus aureus* infections in the United States. JAMA **298:**1763–1771.
9. **Andreini C, Bertini I, Cavallaro G, Holliday GL, Thornton JM.** 2008. Metal ions in biological catalysis: from enzyme databases to general principles. J. Biol. Inorg. Chem. **13:**1205–1218.
10. **Kehl-Fie TE, Skaar EP.** 2010. Nutritional immunity beyond iron: a role for manganese and zinc. Curr. Opin. Chem. Biol. **14:**218–224.
11. **Waldron KJ, Robinson NJ.** 2009. How do bacterial cells ensure that metalloproteins get the correct metal? Nat. Rev. Microbiol. **7:**25–35.
12. **Waldron KJ, Rutherford JC, Ford D, Robinson NJ.** 2009. Metalloproteins and metal sensing. Nature **460:**823–830.
13. **Hood MI, Skaar EP.** 2012. Nutritional immunity: transition metals at the pathogen-host interface. Nat. Rev. Microbiol. **10:**525–537.
14. **Corbin BD, Seeley EH, Raab A, Feldmann J, Miller MR, Torres VJ, Anderson KL, Dattilo BM, Dunman PM, Gerads R, Caprioli RM, Nacken W, Chazin WJ, Skaar EP.** 2008. Metal chelation and inhibition of bacterial growth in tissue abscesses. Science **319:**962–965.
15. **Weinberg ED.** 2009. Iron availability and infection. Biochim. Biophys. Acta **1790:**600–605.
16. **Bullen JJ.** 1981. The significance of iron in infection. Rev. Infect. Dis. **3:**1127–1138.
17. **Weinberg ED.** 1974. Iron and susceptibility to infectious disease. Science **184:**952–956.
18. **Kehl-Fie TE, Chitayat S, Hood MI, Damo S, Restrepo N, Garcia C, Munro KA, Chazin WJ, Skaar EP.** 2011. Nutrient metal sequestration by calprotectin inhibits bacterial superoxide defense, enhancing neutrophil killing of *Staphylococcus aureus*. Cell Host Microbe **10:**158–164.
19. **Yousefi R, Imani M, Ardestani SK, Saboury AA, Gheibi N, Ranjbar B.** 2007. Human calprotectin: effect of calcium and zinc on its secondary and tertiary structures, and role of pH in its thermal stability. Acta Biochim. Biophys. Sin. (Shanghai) **39:**795–802.
20. **Bianchi M, Niemiec MJ, Siler U, Urban CF, Reichenbach J.** 2011. Restoration of anti-*Aspergillus* defense by neutrophil extracellular traps in human chronic granulomatous disease after gene therapy is calprotectin-dependent. J. Allergy Clin. Immunol. **127:**1243–1252.
21. **Hood MI, Mortensen BL, Moore JL, Zhang Y, Kehl-Fie TE, Sugitani N,**

Chazin WJ, Caprioli RM, Skaar EP. 2012. Identification of an *Acinetobacter baumannii* zinc acquisition system that facilitates resistance to calprotectin-mediated zinc sequestration. PLoS Pathog. **8:**e1003068. doi:10.1371/journal.ppat.1003068.

22. **Urban CF, Ermert D, Schmid M, Abu-Abed U, Goosmann C, Nacken W, Brinkmann V, Jungblut PR, Zychlinsky A.** 2009. Neutrophil extracellular traps contain calprotectin, a cytosolic protein complex involved in host defense against *Candida albicans*. PLoS Pathog. **5:**e1000639. doi:10.1371/journal.ppat.1000639.
23. **Liu JZ, Jellbauer S, Poe AJ, Ton V, Pesciaroli M, Kehl-Fie TE, Restrepo NA, Hosking MP, Edwards RA, Battistoni A, Pasquali P, Lane TE, Chazin WJ, Vogl T, Roth J, Skaar EP, Raffatellu M.** 2012. Zinc sequestration by the neutrophil protein calprotectin enhances *Salmonella* growth in the inflamed gut. Cell Host Microbe **11:**227–239.
24. **Clohessy PA, Golden BE.** 1995. Calprotectin-mediated zinc chelation as a biostatic mechanism in host defence. Scand. J. Immunol. **42:**551–556.
25. **Gebhardt C, Nemeth J, Angel P, Hess J.** 2006. S100A8 and S100A9 in inflammation and cancer. Biochem. Pharmacol. **72:**1622–1631.
26. **Brodersen DE, Nyborg J, Kjeldgaard M.** 1999. Zinc-binding site of an S100 protein revealed. Two crystal structures of Ca2+-bound human psoriasin (S100A7) in the Zn2+-loaded and Zn2+-free states. Biochemistry **38:**1695–1704.
27. **Damo SM, Kehl-Fie TE, Sugitani N, Holt ME, Rathi S, Murphy WJ, Zhang Y, Betz C, Hench L, Fritz G, Skaar EP, Chazin WJ.** 2013. Molecular basis for manganese sequestration by calprotectin and roles in the innate immune response to invading bacterial pathogens. Proc. Natl. Acad. Sci. U. S. A. **110:**3841–3846.
28. **Moroz OV, Blagova EV, Wilkinson AJ, Wilson KS, Bronstein IB.** 2009. The crystal structures of human S100A12 in apo form and in complex with zinc: new insights into S100A12 oligomerisation. J. Mol. Biol. **391:**536–551.
29. **Ostendorp T, Diez J, Heizmann CW, Fritz G.** 2011. The crystal structures of human S100B in the zinc- and calcium-loaded state at three pH values reveal zinc ligand swapping. Biochim. Biophys. Acta **1813:**1083–1091.
30. **Damo S, Chazin WJ, Skaar EP, Kehl-Fie TE.** 2012. Inhibition of bacterial superoxide defense: a new front in the struggle between host and pathogen. Virulence **3:**325–328.
31. **Ammendola S, Pasquali P, Pistoia C, Petrucci P, Petrarca P, Rotilio G, Battistoni A.** 2007. High-affinity Zn2+ uptake system ZnuABC is required for bacterial zinc homeostasis in intracellular environments and contributes to the virulence of *Salmonella enterica*. Infect. Immun. **75:**5867–5876.
32. **Campoy S, Jara M, Busquets N, Perez De Rozas AM, Badiola I, Barbe J.** 2002. Role of the high-affinity zinc uptake *znuABC* system in *Salmonella enterica* serovar Typhimurium virulence. Infect. Immun. **70:**4721–4725.
33. **Davis LM, Kakuda T, DiRita VJ.** 2009. A *Campylobacter jejuni znuA* orthologue is essential for growth in low-zinc environments and chick colonization. J. Bacteriol. **191:**1631–1640.
34. **Kim S, Watanabe K, Shirahata T, Watarai M.** 2004. Zinc uptake system (*znuA* locus) of *Brucella abortus* is essential for intracellular survival and virulence in mice. J. Vet. Med. Sci. **66:**1059–1063.
35. **Lewis DA, Klesney-Tait J, Lumbley SR, Ward CK, Latimer JL, Ison CA, Hansen EJ.** 1999. Identification of the *znuA*-encoded periplasmic zinc transport protein of *Haemophilus ducreyi*. Infect. Immun. **67:**5060–5068.
36. **Sabri M, Houle S, Dozois CM.** 2009. Roles of the extraintestinal pathogenic *Escherichia coli* ZnuACB and ZupT zinc transporters during urinary tract infection. Infect. Immun. **77:**1155–1164.
37. **Weston BF, Brenot A, Caparon MG.** 2009. The metal homeostasis protein, Lsp, of *Streptococcus pyogenes* is necessary for acquisition of zinc and virulence. Infect. Immun. **77:**2840–2848.
38. **Anderson ES, Paulley JT, Gaines JM, Valderas MW, Martin DW, Menscher E, Brown TD, Burns CS, Roop RM, Jr.** 2009. The manganese transporter MntH is a critical virulence determinant for *Brucella abortus* 2308 in experimentally infected mice. Infect. Immun. **77:**3466–3474.
39. **Bearden SW, Perry RD.** 1999. The Yfe system of *Yersinia pestis* transports iron and manganese and is required for full virulence of plague. Mol. Microbiol. **32:**403–414.
40. **Berry AM, Paton JC.** 1996. Sequence heterogeneity of PsaA, a 37-kilodalton putative adhesin essential for virulence of *Streptococcus pneumoniae*. Infect. Immun. **64:**5255–5262.
41. **Dintilhac A, Alloing G, Granadel C, Claverys JP.** 1997. Competence and virulence of *Streptococcus pneumoniae*: Adc and PsaA mutants exhibit a requirement for Zn and Mn resulting from inactivation of putative ABC metal permeases. Mol. Microbiol. **25:**727–739.
42. **Horsburgh MJ, Wharton SJ, Cox AG, Ingham E, Peacock S, Foster SJ.** 2002. MntR modulates expression of the PerR regulon and superoxide resistance in *Staphylococcus aureus* through control of manganese uptake. Mol. Microbiol. **44:**1269–1286.
43. **Janulczyk R, Ricci S, Bjorck L.** 2003. MtsABC is important for manganese and iron transport, oxidative stress resistance, and virulence of *Streptococcus pyogenes*. Infect. Immun. **71:**2656–2664.
44. **Sun X, Baker HM, Ge R, Sun H, He Q-Y, Baker EN.** 2009. Crystal structure and metal binding properties of the lipoprotein MtsA, responsible for iron transport in *Streptococcus pyogenes*. Biochemistry **48:**6184–6190.
45. **Papp-Wallace KM, Maguire ME.** 2006. Manganese transport and the role of manganese in virulence. Annu. Rev. Microbiol. **60:**187–209.
46. **Perry RD, Mier I, Jr, Fetherston JD.** 2007. Roles of the Yfe and Feo transporters of *Yersinia pestis* in iron uptake and intracellular growth. Biometals **20:**699–703.
47. **Hantke K.** 2005. Bacterial zinc uptake and regulators. Curr. Opin. Microbiol. **8:**196–202.
48. **Hazlett KR, Rusnak F, Kehres DG, Bearden SW, La Vake CJ, La Vake ME, Maguire ME, Perry RD, Radolf JD.** 2003. The *Treponema pallidum* tro operon encodes a multiple metal transporter, a zinc-dependent transcriptional repressor, and a semi-autonomously expressed phosphoglycerate mutase. J. Biol. Chem. **278:**20687–20694.
49. **Lawrence MC, Pilling PA, Epa VC, Berry AM, Ogunniyi AD, Paton JC.** 1998. The crystal structure of pneumococcal surface antigen PsaA reveals a metal-binding site and a novel structure for a putative ABC-type binding protein. Structure **6:**1553–1561.
50. **Lee YH, Dorwart MR, Hazlett KRO, Deka RK, Norgard MV, Radolf JD, Hasemann CA.** 2002. The crystal structure of Zn(II)-free *Treponema pallidum* TroA, a periplasmic metal-binding protein, reveals a closed conformation. J. Bacteriol. **184:**2300–2304.
51. **McDevitt CA, Ogunniyi AD, Valkov E, Lawrence MC, Kobe B, McEwan AG, Paton JC.** 2011. A molecular mechanism for bacterial susceptibility to zinc. PLoS Pathog. **7:**e1002357. doi:10.1371/journal.ppat.1002357.
52. **Anderson AS, Scully IL, Timofeyeva Y, Murphy E, McNeil LK, Mininni T, Nunez L, Carriere M, Singer C, Dilts DA, Jansen KU.** 2012. *Staphylococcus aureus* manganese transport protein C is a highly conserved cell surface protein that elicits protective immunity against *S. aureus* and *Staphylococcus epidermidis*. J. Infect. Dis. **205:**1688–1696.
53. **Cockayne A, Hill PJ, Powell NB, Bishop K, Sims C, Williams P.** 1998. Molecular cloning of a 32-kilodalton lipoprotein component of a novel iron-regulated *Staphylococcus epidermidis* ABC transporter. Infect. Immun. **66:**3767–3774.
54. **Bae T, Schneewind O.** 2006. Allelic replacement in *Staphylococcus aureus* with inducible counter-selection. Plasmid **55:**58–63.
55. **Grossoehme N, Kehl-Fie TE, Ma Z, Adams KW, Cowart DM, Scott RA, Skaar EP, Giedroc DP.** 2011. Control of copper resistance and inorganic sulfur metabolism by paralogous regulators in *Staphylococcus aureus*. J. Biol. Chem. **286:**13522–13531.
56. **Kehl-Fie TE, Porsch EA, Miller SE, St Geme JW, III.** 2009. Expression of *Kingella kingae* type IV pili is regulated by sigma54, PilS, and PilR. J. Bacteriol. **191:**4976–4986.
57. **Karavolos MH, Horsburgh MJ, Ingham E, Foster SJ.** 2003. Role and regulation of the superoxide dismutases of *Staphylococcus aureus*. Microbiology **149:**2749–2758.
58. **Valderas MW, Hart ME.** 2001. Identification and characterization of a second superoxide dismutase gene (*sodM*) from *Staphylococcus aureus*. J. Bacteriol. **183:**3399–3407.
59. **Gu M, Imlay JA.** 2011. The SoxRS response of *Escherichia coli* is directly activated by redox-cycling drugs rather than by superoxide. Mol. Microbiol. **79:**1136–1150.
60. **Hassan HM, Fridovich I.** 1979. Paraquat and *Escherichia coli*. Mechanism of production of extracellular superoxide radical. J. Biol. Chem. **254:**10846–10852.
61. **Attia AS, Schroeder KA, Seeley EH, Wilson KJ, Hammer ND, Colvin DC, Manier ML, Nicklay JJ, Rose KL, Gore JC, Caprioli RM, Skaar EP.** 2012. Monitoring the inflammatory response to infection through the integration of MALDI IMS and MRI. Cell Host Microbe **11:**664–673.
62. **Becker JS, Breuer U, Hsieh HF, Osterholt T, Kumtabtim U, Wu B, Matusch A, Caruso JA, Qin Z.** 2010. Bioimaging of metals and biomolecules in mouse heart by laser ablation inductively coupled plasma mass

spectrometry and secondary ion mass spectrometry. Anal. Chem. **82:** 9528–9533.
63. **Becker JS, Matusch A, Palm C, Salber D, Morton KA.** 2010. Bioimaging of metals in brain tissue by laser ablation inductively coupled plasma mass spectrometry (LA-ICP-MS) and metallomics. Metallomics **2:**104–111.
64. **Caprioli RM, Farmer TB, Gile J.** 1997. Molecular imaging of biological samples: localization of peptides and proteins using MALDI-TOF MS. Anal. Chem. **69:**4751–4760.
65. **Chaurand P, Sanders ME, Jensen RA, Caprioli RM.** 2004. Proteomics in diagnostic pathology: profiling and imaging proteins directly in tissue sections. Am. J. Pathol. **165:**1057–1068.
66. **Matusch A, Depboylu C, Palm C, Wu B, Hoglinger GU, Schafer MK, Becker JS.** 2010. Cerebral bioimaging of Cu, Fe, Zn, and Mn in the MPTP mouse model of Parkinson's disease using laser ablation inductively coupled plasma mass spectrometry (LA-ICP-MS). J. Am. Soc. Mass Spectrom. **21:**161–171.
67. **Hobbs JA, May R, Tanousis K, McNeill E, Mathies M, Gebhardt C, Henderson R, Robinson MJ, Hogg N.** 2003. Myeloid cell function in MRP-14 (S100A9) null mice. Mol. Cell. Biol. **23:**2564–2576.
68. **Prohaska JR, Lukasewycz OA.** 1981. Copper deficiency suppresses the immune response of mice. Science **213:**559–561.
69. **White C, Lee J, Kambe T, Fritsche K, Petris MJ.** 2009. A role for the ATP7A copper-transporting ATPase in macrophage bactericidal activity. J. Biol. Chem. **284:**33949–33956.
70. **Arredondo M, Nunez MT.** 2005. Iron and copper metabolism. Mol. Aspects Med. **26:**313–327.
71. **Edvinsson M, Frisk P, Molin Y, Hjelm E, Ilback NG.** 2008. Trace element balance is changed in infected organs during acute *Chlamydophila pneumoniae* infection in mice. Biometals **21:**229–237.
72. **Cassat JE, Skaar EP.** 2012. Metal ion acquisition in *Staphylococcus aureus*: overcoming nutritional immunity. Semin. Immunopathol. **34:** 215–235.
73. **Wintergerst ES, Maggini S, Hornig DH.** 2007. Contribution of selected vitamins and trace elements to immune function. Ann. Nutr. Metab. **51:** 301–323.